Scientific Research Publishing

Open Journal of Applied Sciences, 2018, 8, 170-183
http://www.scirp.org/journal/ojapps
ISSN Online: 2165-3925
ISSN Print: 2165-3917

Lock-in-Amplifier Model for Analyzing the Behavior of Signal Harmonics in Magnetic Particle Imaging

Kenya Murase[1,2*], Kazuki Shimada[1]

[1]Department of Medical Physics and Engineering, Division of Medical Technology and Science, Faculty of Health Science, Graduate School of Medicine, Osaka University, Suita, Japan
[2]Global Center for Medical Engineering and Informatics, Osaka University, Suita, Japan
Email: *murase@sahs.med.osaka-u.ac.jp

How to cite this paper: Murase, K. and Shimada, K. (2018) Lock-in-Amplifier Model for Analyzing the Behavior of Signal Harmonics in Magnetic Particle Imaging. *Open Journal of Applied Sciences*, **8**, 170-183.
https://doi.org/10.4236/ojapps.2018.85014

Received: April 27, 2018
Accepted: May 28, 2018
Published: May 31, 2018

Abstract

The purpose of this study was to present a lock-in-amplifier model for analyzing the behavior of signal harmonics in magnetic particle imaging (MPI) and some simulation results based on this model. In the lock-in-amplifier model, the signal induced by magnetic nanoparticles (MNPs) in a receiving coil was multiplied with a reference signal, and was then fed through a low-pass filter to extract the DC component of the signal (output signal). The MPI signal was defined as the mean of the absolute value of the output signal. The magnetization and particle size distribution of MNPs were assumed to obey the Langevin theory of paramagnetism and a log-normal distribution, respectively, and the strength of the selection magnetic field (SMF) in MPI was assumed to be given by the product of the gradient strength of the SMF and the distance from the field-free region (x). In addition, Gaussian noise was added to the signal induced by MNPs using normally-distributed random numbers. The relationships between the MPI signal and x were calculated for the odd- and even-numbered harmonics and were investigated for various time constants of the low-pass filter used in the lock-in amplifier and particle sizes and their distributions of MNPs. We found that the behavior of the MPI signal largely depended on the time constant of the low-pass filter and the particle size of MNPs. This lock-in-amplifier model will be useful for better understanding, optimizing, and developing MPI, and for designing MNPs appropriate for MPI.

Keywords

Magnetic Particle Imaging (MPI), Lock-in-Amplifier Model, Signal Harmonics, Magnetic Nanoparticles (MNPs)

1. Introduction

In 2005, a new imaging method called magnetic particle imaging (MPI) was introduced [1]. MPI allows for imaging of the spatial distribution of magnetic nanoparticles (MNPs) with high sensitivity, high spatial resolution, and high imaging speed.

MPI utilizes the nonlinear response of MNPs to detect their presence in an alternating magnetic field called the drive magnetic field. Spatial encoding is accomplished by saturating the magnetization of the MNPs almost everywhere except in the vicinity of a special region called the field-free point (FFP) or field-free line (FFL) using a static magnetic field called the selection magnetic field [1].

Due to the nonlinear response of the MNPs to an applied drive magnetic field, the signals generated by the MNPs in a receiving coil contain not only the excitation frequency but also the harmonics of this frequency. These harmonics are used for image reconstruction in MPI [1]. Thus, the qualitative and quantitative properties of MPI directly depend on the characteristics of these harmonics. It is also known that the magnetization response of MNPs depends not only on the magnetic properties of MNPs but also on the particle size and distribution of MNPs [2].

For a better understanding and optimization of MPI, it is important to investigate the behavior of signal harmonics generated by MNPs under various conditions of the drive and selection magnetic fields and their dependence on the particle size and distribution of MNPs. We previously investigated the behavior of signal harmonics in MPI by experimental and simulation studies, and reported that it largely depended on the strength of the drive and selection magnetic fields and the particle size distribution of MNPs [3]. In our previous studies, signal harmonics were calculated from the spectra obtained by the Fourier transformation of the signals induced by MNPs in a receiving coil [3].

Lock-in amplifiers were invented in the early 1940s to extract electrical signals in extremely noisy environments [4]. They employ a homodyne detection scheme and low-pass filtering to measure the electrical signal relative to a periodic reference signal. They extract signals in a defined frequency band around the reference frequency, efficiently rejecting all other frequency components. They are also often used to extract signals in the field of MPI [5] [6].

The purpose of this study was to present a lock-in-amplifier model for analyzing the behavior of signal harmonics in MPI and some simulation results based on this model.

2. Materials and Methods

2.1. Lock-in-Amplifier Model

Figure 1 illustrates a lock-in-amplifier model. A lock-in amplifier performs a multiplication of its input with a reference signal, and then applies an adjustable low-pass filter to the result. The multiplication is called "signal mixing", as illustrated

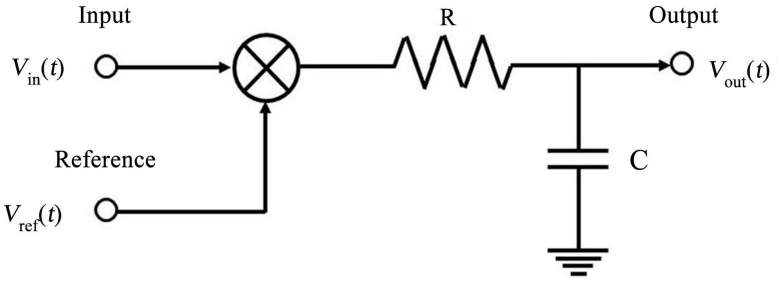

Figure 1. Illustration of a lock-in-amplifier model. The input signal $\left[v_{in}(t)\right]$ is multiplied by the reference signal $\left[v_{ref}(t)\right]$ and then the mixed signal $\left[v_{mix}(t)\right]$ is low-pass filtered to reject the noise and finally converted to the output signal $\left[v_{out}(t)\right]$.

by $\otimes$ in **Figure 1**. The signal mixing is mathematically expressed as a multiplication of the input signal $\left[v_{in}(t)\right]$ with the complex reference signal $\left[v_{ref}(t)\right]$, which is given by

$$v_{mix}(t) = v_{in}(t) \cdot v_{ref}(t) \tag{1}$$

where $v_{mix}(t)$ denotes the signal after mixing and $v_{ref}(t)$ is given by

$$v_{ref}(t) = \sqrt{2}\mathrm{e}^{-j2\pi f_{ref} t} \tag{2}$$

In Equation (2), $j = \sqrt{-1}$ and f_{ref} denotes the frequency of the reference signal. The mixed signal is then fed through a low-pass filter to extract the DC component of the signal. Mathematically, this procedure is given by

$$V_{out}(f) = V_{mix}(f) \cdot H_{LPF}(f) \tag{3}$$

where $V_{out}(f)$ and $V_{mix}(f)$ denote the Fourier transforms ($\mathcal{F}$) of the output signal $\left[v_{out}(t)\right]$ and $v_{mix}(t)$, respectively, *i.e.*, $V_{out}(f) = \mathcal{F}\left[v_{out}(t)\right]$ and $V_{mix}(f) = \mathcal{F}\left[v_{mix}(t)\right]$. $H_{LPF}(f)$ denotes the transfer function of the first-order RC low-pass filter and is well approximated by

$$H_{LPF}(f) = \frac{1}{1 + j2\pi f\tau} \tag{4}$$

where $\tau = RC$ is the filter time constant with resistance R and capacitance C (**Figure 1**). It is well known that the unit step response of the first-order RC low-pass filter in the time domain $\left[R_{STEP}(t)\right]$ is given by

$$R_{STEP}(t) = 1 - \mathrm{e}^{-\frac{t}{\tau}} \tag{5}$$

Figure 2(a) and **Figure 2(b)** show $H_{LPF}(f)$ in a Bode plot, *i.e.*, $20\log_{10}\left|H_{LPF}(f)\right|$ as a function of $\log_{10}(f)$ and $R_{STEP}(t)$ for various τ values, respectively. $v_{out}(t)$ is obtained by the inverse Fourier transformation ($\mathcal{F}^{-1}$) of $V_{out}(f)$, *i.e.*, $v_{out}(t) = \mathcal{F}^{-1}\left[V_{out}(f)\right]$ and is given by

$$v_{out}(t) = \left|v_{out}(t)\right| \mathrm{e}^{j\phi(t)} \tag{6}$$

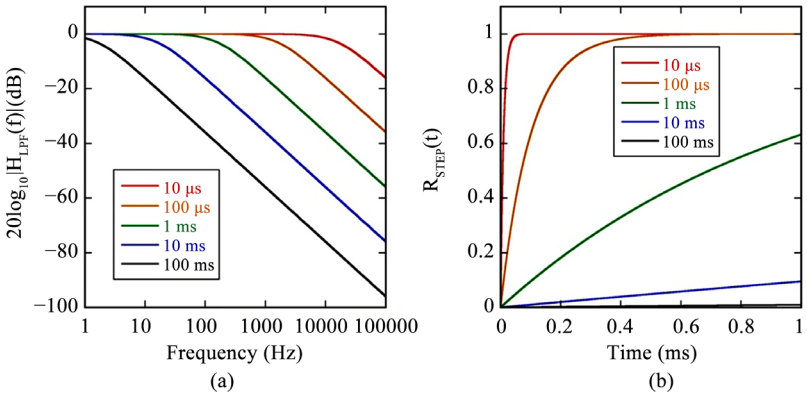

Figure 2. (a) Transfer function of the first-order RC low-pass filter $\left[H_{LPF}(f)\right]$ given by Equation (4) in a Bode plot, *i.e.*, $20\log_{10}\left|H_{LPF}(f)\right|$ as a function of $\log_{10}(f)$, for various values of the time constant of the low-pass filter used in the lock-in amplifier (τ); (b) Unit step response of the first-order RC low-pass filter in the time domain given by Equation (5) for various τ values.

where $\left|v_{out}(t)\right|$ and $\phi(t)$ denote the absolute value of $v_{out}(t)$ and phase at time *t*, respectively. In this study, the MPI signal (S_{MPI}) is defined as the mean of $\left|v_{out}(t)\right|$, *i.e.*,

$$S_{MPI} = \overline{\left|v_{out}(t)\right|} \tag{7}$$

2.2. Signals Induced by MNPs

Assuming a single receiving coil with sensitivity $\left[\sigma_{rx}(\boldsymbol{r})\right]$ at spatial position $\boldsymbol{r}$, the changing magnetization induces a voltage according to Faraday's law $\left[v_{rx}(t)\right]$, which is given by [7]

$$v_{rx}(t) = -\mu_0 \frac{\mathrm{d}}{\mathrm{d}t}\int_{\Omega}\sigma_{rx}(\boldsymbol{r})C(\boldsymbol{r})M(\boldsymbol{r},t)\mathrm{d}r \tag{8}$$

where Ω denotes the volume containing MNPs, $C(\boldsymbol{r})$ is the concentration of MNPs at position $\boldsymbol{r}$, $M(\boldsymbol{r},t)$ is the magnetization at position $\boldsymbol{r}$ and time *t*, and μ_0 is the magnetic permeability of a vacuum. $\sigma_{rx}(\boldsymbol{r})$ is the receiving coil sensitivity derived from the magnetic field that the coil would produce if driven with a unit current [7].

In the following, the receiving coil sensitivity is assumed to be constant and uniform over the volume of interest and is denoted by σ_0. When we consider the signal generated by a point-like distribution of MNPs, that is, the MNP distribution is approximated by Dirac's δ function such that $C(\boldsymbol{r}) = C_0\delta(\boldsymbol{r})$ with C_0 being constant, the volume integral in Equation (8) vanishes and $v_{rx}(t)$ given by Equation (8) is reduced to

$$v_{rx}(t) = -\mu_0\sigma_0 C_0 \frac{\mathrm{d}M(t)}{\mathrm{d}t} \tag{9}$$

Note that $M(0,t)$ is denoted by $M(t)$ in Equation (9) for simplicity. We can

neglect constant factors in Equation (9).

In addition, we assume that the signal obtained by the receiving coil includes Gaussian white noise [8]. Thus, the input signal to a lock-in amplifier [$v_{in}(t)$ in Figure 1] is calculated by

$$v_{in}(t) = v_{rx}(t) + \sqrt{\frac{\overline{v_{rx}(t)^2}}{SNR}} \cdot randn \tag{10}$$

where $\overline{v_{rx}(t)^2}$, *randn*, and *SNR* denote the mean of $v_{rx}(t)^2$, a normally-distributed random number with zero mean and unit variance, and signal-to-noise ratio, respectively.

2.3. Langevin Function

Assuming that MNPs are in equilibrium, the magnetization of MNPs in response to an applied magnetic field can be described by the Langevin function [9], which is given by

$$M(\xi) = M_0\left(\coth\xi - \frac{1}{\xi}\right) \tag{11}$$

where M_0 is the saturation magnetization and ξ is the ratio of the magnetic energy of a particle with magnetic moment m in an external magnetic field H to the thermal energy given by the Boltzmann constant k_B and the absolute temperature T:

$$\xi = \frac{\mu_0 mH}{k_B T} = \frac{\mu_0 M_d V_M H}{k_B T} \tag{12}$$

In Equation (12), M_d is the domain magnetization of a suspended particle, and V_M is the magnetic volume given by $V_M = \pi D^3/6$ for a particle of diameter D.

In this study, we assume that the external magnetic field at position x and time t $\left[H(x,t)\right]$ is given by

$$H(x,t) = H_s(x) + H_D(t) \tag{13}$$

where $H_s(x)$ is the strength of the selection magnetic field at position x and $H_D(t)$ is the strength of the drive magnetic field at time t. We also assume that $H_D(t)$ is given by

$$H_D(t) = H_{DMF}\cos(2\pi f_{DMF} t) \tag{14}$$

where H_{DMF} and f_{DMF} denote the amplitude and frequency of the drive magnetic field, respectively. Furthermore, we assume that $H_s(x)$ is given by

$$H_s(x) = G_x \cdot x \tag{15}$$

where G_x and x denote the gradient strength of the selection magnetic field and the distance from the field-free region, respectively.

2.4. Particle Size Distribution

When the particle size distribution obeys a log-normal distribution [10], the

magnetization of MNPs averaged based on this particle size distribution $\left(\langle M \rangle\right)$ is given by [3]

$$\langle M \rangle = \frac{1}{\sqrt{2\pi}} \int_0^\infty \frac{M(D)}{\sigma D} \exp\left[-\frac{1}{2} \left(\frac{\ln(D) - \mu}{\sigma} \right)^2 \right] \mathrm{d}D \tag{16}$$

where $M(D)$ denotes the magnetization of MNPs with diameter D. μ and σ denote the mean and standard deviation (SD) of the log-normal distribution, respectively [3]. It should be noted that the relationships between μ and D and between σ and D are represented by

$$\mu = \ln\left[\mathrm{E}(D) \right] - \frac{1}{2} \ln\left[\frac{\mathrm{Var}(D)}{\mathrm{E}^2(D)} + 1 \right] \tag{17}$$

and

$$\sigma = \sqrt{\ln\left[\frac{\mathrm{Var}(D)}{\mathrm{E}^2(D)} + 1 \right]} \tag{18}$$

respectively, where $\mathrm{E}(D)$ and $\mathrm{Var}(D)$ denote the expectation and variance of D, respectively.

2.5. Simulation Studies

In this study, we considered magnetite (Fe_3O_4) as MNPs, and M_d in Equation (11) was taken as 446 kA/m [3]. The amplitude and frequency of the drive magnetic field [H_{DMF} and f_{DMF} in Equation (14), respectively] were fixed at 10 mT and 400 Hz, respectively [5] [6], and the temperature was assumed to be room temperature (293.15 K) in all simulation studies. Since the frequency of the drive magnetic field was fixed at 400 Hz as described above, the third-harmonic MPI signal corresponds to the S_{MPI} value given by Equation (7) at $f_{ref} = 1200$ Hz.

Unless specifically stated, $\mathrm{E}(D)$ and σ in Equation (17) and Equation (18) were assumed to be 20 nm and 0.2, respectively, and G_x in Equation (15) was assumed to be 2 T/m. When investigating the dependence of the odd- and even-numbered harmonics on the selection magnetic field, G_x in Equation (15) was varied from 1 to 5 T/m. When investigating the dependence of the third-harmonic signal on the particle size of MNPs, $\mathrm{E}(D)$ and σ in Equation (17) and Equation (18) were varied from 10 to 50 nm and from 0.05 to 0.4, respectively.

3. Results

Figure 3(a) and **Figure 3(b)** show examples of $v_{in}(t)$ and $v_{ref}(t)$, respectively. **Figure 3(c)** shows $\left|v_{out}(t)\right|$ obtained from $v_{in}(t)$ and $v_{ref}(t)$ by the inverse Fourier transformation of $V_{out}(f)$ given by Equation (3). In these cases, the MNPs were assumed to be located at the center of the field-free region, *i.e.*, $x = 0$. f_{ref} was taken as 1200 Hz. The time constant of the low-pass filter used in the lock-in amplifier (τ) and *SNR* were assumed to be 10 ms and 20, respectively.

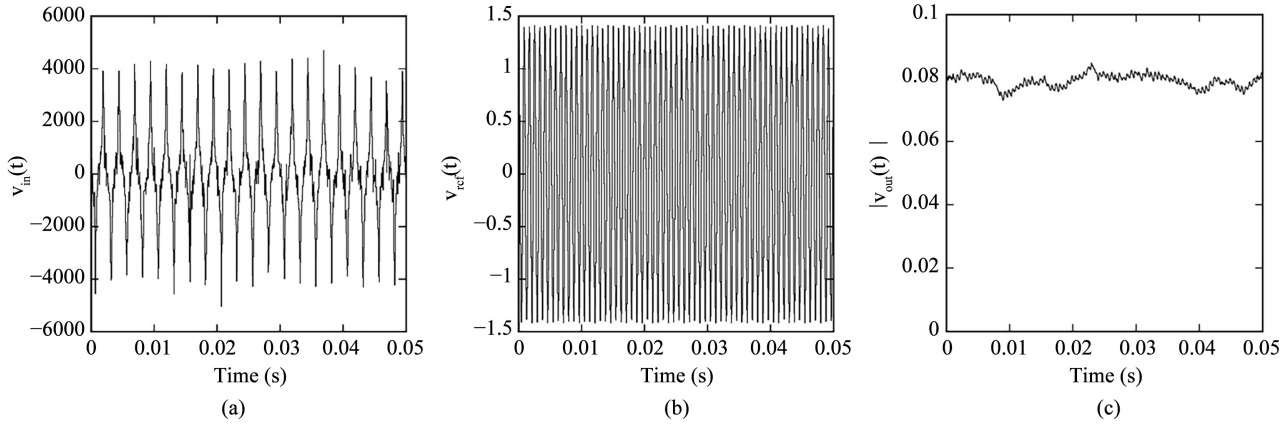

Figure 3. (a) Example of $v_{in}(t)$; (b) Example of $v_{ref}(t)$; (c) $|v_{out}(t)|$ obtained from $v_{in}(t)$ and $v_{ref}(t)$ by the inverse Fourier transformation of $V_{out}(f)$ given by Equation (3).

Figure 4 shows the relationship between the MPI signal given by Equation (7) (S_{MPI}) and the distance from the field-free region (x) for the odd-numbered harmonics, whereas **Figure 5** shows those for the even-numbered harmonics. In these cases, the gradient strength of the selection magnetic field [G_x in Equation (15)] was taken as 2 T/m. As in **Figure 3**, τ and *SNR* were assumed to be 10 ms and 20, respectively. As shown in **Figure 4** and **Figure 5**, the odd-numbered harmonics are not zero at $x = 0$, whereas the even-numbered harmonics are zero at $x = 0$. The S_{MPI} value at the peak for the third-harmonic signal was the largest of the studied odd-numbered harmonics and that for the second-harmonic signal was the largest of the studied even-numbered harmonics. As shown in **Figure 5**, the oscillation including the dent characteristic of each harmonic signal was observed and the number of the dent increased with increasing order of the harmonics for both the odd- and even-numbered harmonics.

Figure 6 shows the relationship between the third-harmonic MPI signal, *i.e.*, S_{MPI} at $f_{ref} = 1200$ Hz and x when G_x was varied from 1 to 5 T/m. The other parameters were the same as in **Figure 4** and **Figure 5**. As shown in **Figure 6**, the plot of S_{MPI} versus x was scaled by a factor of G_x in the x axis, because $H_s(x)$ was assumed to be proportional to G_x as given by Equation (15).

Figure 7 shows the relationship between the third-harmonic MPI signal and x when τ was varied from 10 μs to 100 ms, whereas the other parameters were the same as in **Figure 6**. As shown in **Figure 7**, the dent at $x \approx 0.3$ cm decreased with increasing τ value.

Figure 8 shows the coefficient of variation (CV) of the third-harmonic MPI signal as a function of τ for various SNR values of the input signal. It should be noted that the CV is defined as the ratio of the SD to the mean value. **Figure 8(a)** shows the case for x of 0 cm, and **Figure 8(b)** the case for x of 1 cm. The CV value decreased with increasing τ value. When $x = 0$ [**Figure 8(a)**], the dependency on SNR was smaller than when $x \neq 0$ [**Figure 8(b)**].

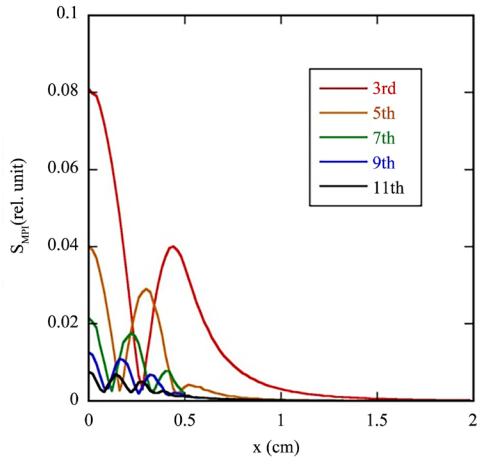

Figure 4. Relationship between the MPI signal (S_{MPI}) given by Equation (7) and the distance from the field-free region (x) for the odd-numbered harmonics in the case when the gradient strength of the selection magnetic field (G_x) is 2 T/m.

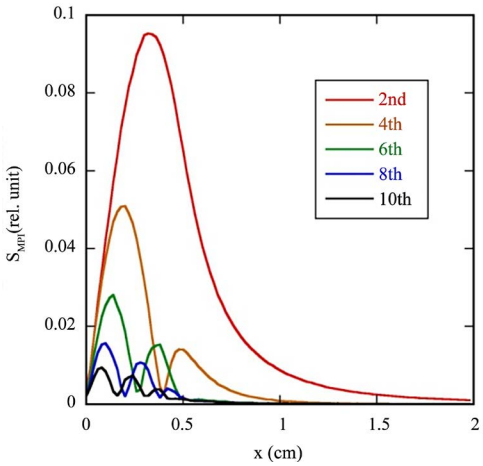

Figure 5. Relationship between S_{MPI} and x for the even-numbered harmonics in the case when G_x is 2 T/m.

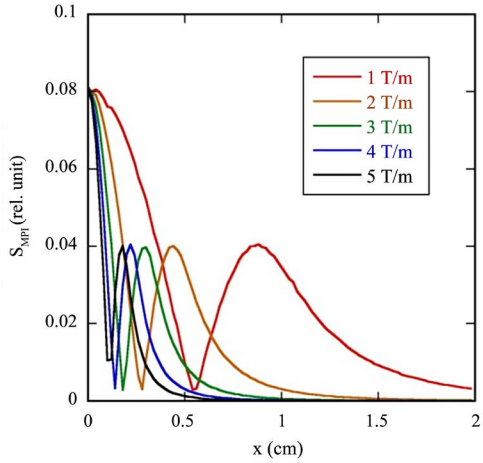

Figure 6. Relationship between the third-harmonic MPI signal, *i.e.*, S_{MPI} at $f_{ref} = 1200$ Hz and x when G_x was varied from 1 to 5 T/m.

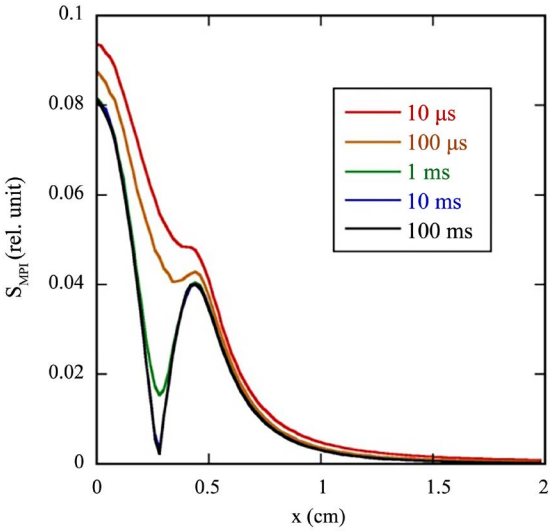

Figure 7. Relationship between the third-harmonic MPI signal and x when τ was varied from 10 μs to 100 ms.

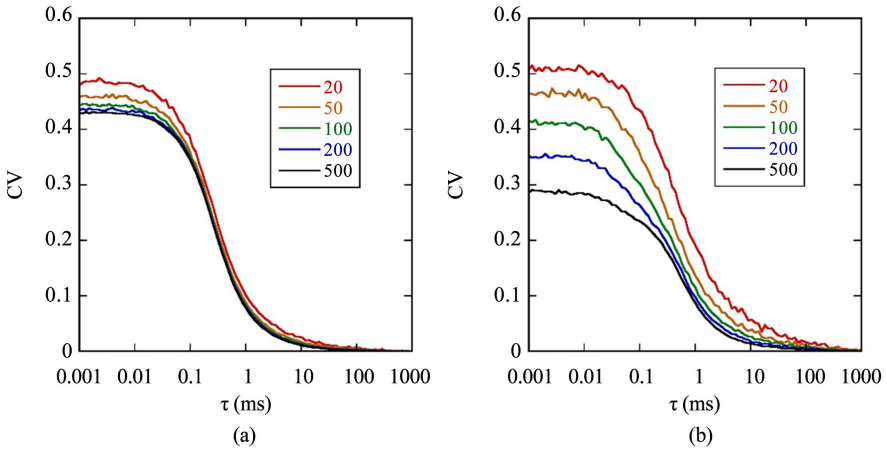

Figure 8. Coefficient of variation (CV) of the third-harmonic MPI signal as a function of τ for various signal-to-noise (SNR) values of $v_{in}(t)$. (a) is the case for x of 0 cm; and (b) is the case for x of 1 cm.

Figure 9 shows a comparison of the relationship between S_{MPI} and x when the third harmonics alone and multiple odd-numbered harmonics were used. The S_{MPI} value at $x=0$ increased and the dent at $x \approx 0.3$ cm decreased as the number of added odd-numbered harmonics increased.

Figure 10 shows a comparison of the relationship between the third-harmonic MPI signal and x when $\mathrm{E}(D)$ in Equation (17) was varied from 10 to 50 nm. As shown in **Figure 10**, the third-harmonic MPI signal largely depended on $\mathrm{E}(D)$ of MNPs.

Figure 11 shows a comparison of the relationship between the third-harmonic MPI signal and x when the σ value given by Equation (18) was varied from 0.05 to 0.4. Although the third-harmonic MPI signal also depended on σ, its effect was much smaller than that of $\mathrm{E}(D)$ (**Figure 10**).

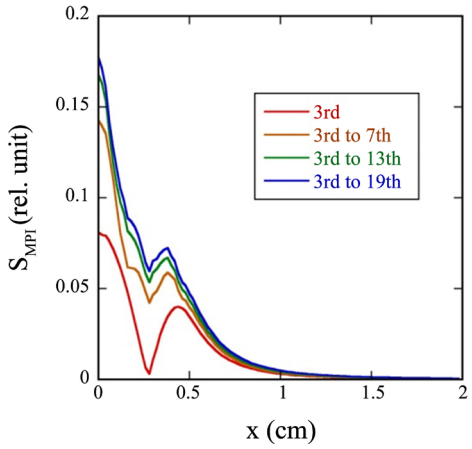

Figure 9. Relationship between S_{MPI} and x when only the third-harmonic signal or multiple odd-numbered harmonics were used. The red, yellow, green, and blue curves represent cases when only the third-harmonic signal was used, the third- to 7th-harmonic signals were added, the third- to 13th-harmonic signals were added, and the third- to 19th-harmonic signals were added, respectively.

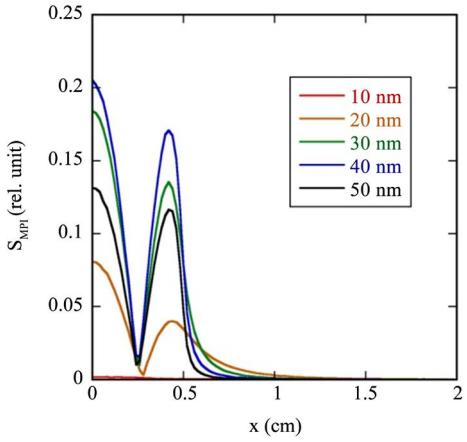

Figure 10. Relationship between the third-harmonic MPI signal and $\boldsymbol{x}$ when $\mathbf{E}(\boldsymbol{D})$ in Equation (17) was varied from 10 to 50 nm.

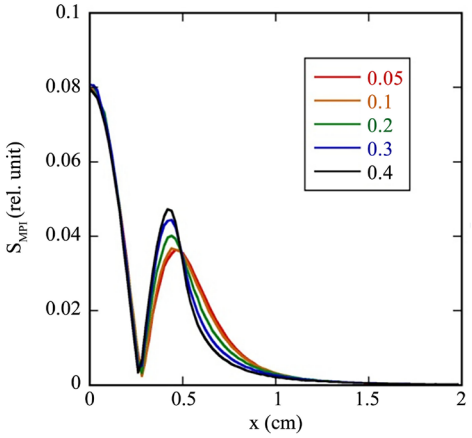

Figure 11. Relationship between the third-harmonic MPI signal and x when the σ value given by Equation (18) was varied from 0.05 to 0.4.

4. Discussion

We previously investigated the behavior of signal harmonics in MPI and reported that the behavior of the odd- and even-numbered harmonics of MPI signals largely depends not only on the strength of the drive and selection magnetic fields but also on the particle size distribution of MNPs [3]. In our previous study, the signal harmonics were calculated from the spectra obtained by the Fourier transformation of the signal generated by MNPs in a receiving coil [3]. In considering the practical application of MPI, it would be important to distinguish the signals generated by the MNPs from those induced by the receiving coil itself and to remove this feed through interference [3] [5] [6]. Furthermore, it would be important to increase the SNR of MPI signals, especially when the SNR is low.

Lock-in amplifiers are often used to extract signals in MPI [5] [6] because they are effective for extracting signals in extremely noisy environments [4]. In this paper, we presented a lock-in-amplifier model for analyzing the behavior of signal harmonics in MPI and some simulation results based on this model (**Figures 4-11**). Our results demonstrated that the behavior of the MPI signals depends on the parameters in the lock-in amplifier such as the time constant of the low-pass filter (**Figure 7** and **Figure 8**).

We simulated the magnetization of MNPs in response to the drive magnetic field by using the Langevin function given by Equation (11). This is one of the most extensively studied models in MPI and is based on the assumption that MNPs are in equilibrium [11]. This appears to be valid at the low frequency of the drive magnetic field where the magnetization of MNPs is in equilibrium. As the frequency of the drive magnetic field increases, a relaxation time governs the ability of MNPs to follow changes in the drive magnetic field via two distinct relaxation mechanisms; the Néel and Brownian mechanisms [12]. In the Néel mechanism, internal reorientation of the magnetic moment of MNPs occurs, whereas physical rotation of MNPs occurs in the Brownian mechanism, and its characteristic time (τ_B) is proportional to the viscosity of the suspending solvent [12]. As previously described, the frequency of the drive magnetic field was set at 400 Hz in this study, which is much lower than the reciprocal of τ_B. Thus, the effect of viscosity appears to be negligible in this study. When this effect cannot be neglected, however, it would be necessary to perform more detailed analysis based on the stochastic Langevin equation considering Néel relaxation and Brownian rotation simultaneously [11] [13].

Because not all particles in a certain volume have the same diameter D, the magnetization of MNPs should be averaged based on the particle size distribution. The result of a natural growth process during particle synthesis does not yield particles with a single diameter D, but particles with a polydispersed particle size distribution [10]. A reasonable and commonly used approach for modeling is the log-normal distribution [10]. Thus, we assumed that the particle size distribution obeys a log-normal distribution [10]. In this case, the averaged

magnetization of MNPs $\left(\langle M \rangle\right)$ is given by Equation (16).

Theoretically, the odd-numbered harmonics should not be zero, whereas the even-numbered harmonics should be zero when the selection magnetic field is not applied, *i.e.*, at the center of the field-free region such as FFP or FFL [3]. Our results (**Figure 4** and **Figure 5**) showed that the odd-numbered harmonics were not zero and even-numbered harmonics were almost zero at $x = 0$, as expected theoretically [3]. These results are also consistent with those previously obtained experimentally [3]. Furthermore, the third-harmonic signal was the largest of the studied odd-numbered harmonics (**Figure 4**). As previously described, the odd-numbered harmonics are generally used for image reconstruction in MPI [1] because their signals appear at the field-free region and decrease while oscillating outside the field-free region as shown in **Figure 4**, from which the spatial distribution of MNPs can be encoded. Since the third-harmonic signal at the center of the field-free region is the largest of the odd-numbered harmonics except for the first-harmonic signal as shown in **Figure 4**, it is commonly exploited for image reconstruction in MPI [5] [6].

The relationship between the MPI signal [S_{MPI} given by Equation (7)] and the distance from the field-free region (x) [**Figure 4**, **Figure 6**, **Figure 7**, and **Figures 9-11**] appears to correspond to the system function in the spatial domain in MPI. In projection-based MPI [5] [6] [14], the projection data are considered to be given by the convolution between the line integral of the concentration of MNPs through the FFL and the system function in the spatial domain, implying that the quantitative property of MPI can be enhanced by deconvolution of the system function from the projection data [14].

As shown in **Figure 7**, the relationship between the MPI signal and x largely depended on the τ value in the low-pass filter [Equation (4)]. The dent at $x \approx 0.3$ cm decreased with decreasing τ value. This appears to be mainly due to the increase in contamination of harmonics other than the third harmonics. In contrast, the CV value increased with decreasing τ value (**Figure 8**). Furthermore, as shown in **Figure 2(b)**, the delay in the unit step response increases with increasing τ value, which will cause blurring in MPI [14]. Thus, it is important to select an appropriate value for τ in the low-pass filter by taking these factors into consideration.

As shown in **Figure 9**, when using multiple odd-numbered harmonics, the MPI signal at the center of the field-free region, *i.e.*, $x = 0$ was greater by a factor of approximately 2 compared to the case when only the third-harmonic signal was used, suggesting that the sensitivity of MPI can be increased by using multiple odd-numbered harmonics. Furthermore, when using multiple odd-numbered harmonics, the dent at $x \approx 0.3$ cm decreased, which was observed when only the third-harmonic signal was used. These findings appear to be advantageous in correcting for the system function in the spatial domain and/or for reducing artifacts induced by such a dent, because the system function in the spatial domain can be approximated by a smoothly-changing function such as the Gaussian function.

We used the first-order RC low-pass filter for extracting the DC component of the signal after mixing (**Figure 1**), because it is one of the simplest low-pass filters. The transfer function and unit step response of this filter are shown for various τ values in **Figure 2(a)** and **Figure 2(b)**, respectively. When steeper roll-offs towards higher frequencies are desired, they can be achieved by cascading multiple first-order RC low-pass filters, *i.e.*, the higher-order RC low-pass filter.

As previously described, we defined the MPI signal as the mean of $\left|v_{out}(t)\right|$ [Equation (7)] and did not consider the phase [$\phi(t)$ in Equation (6)] in this study. Lock-in amplifiers are also used as phase-shift detectors [15] and $\phi(t)$ can be calculated from

$$\phi(t) = \tan^{-1} \frac{\mathrm{Im}\left\lfloor v_{out}(t) \right\rfloor}{\mathrm{Re}\left\lfloor v_{out}(t) \right\rfloor} \tag{19}$$

where $\mathrm{Re}\left\lfloor v_{out}(t) \right\rfloor$ and $\mathrm{Im}\left\lfloor v_{out}(t) \right\rfloor$ denote the real and imaginary parts of $v_{out}(t)$, respectively. Actually, $\mathrm{Re}\left\lfloor v_{out}(t) \right\rfloor$ and $\mathrm{Im}\left\lfloor v_{out}(t) \right\rfloor$ are detected using phase shifters in lock-in amplifiers [15]. It may also be useful to investigate the dependency of $\phi(t)$ on the strength of the drive and selection magnetic fields and the particle size distribution of MNPs for analyzing the behavior of signal harmonics in MPI. Such a study is currently in progress.

5. Conclusion

We presented a lock-in-amplifier model for analyzing the behavior of signal harmonics in MPI and some simulation results based on this model. This model will be useful for better understanding, optimizing, and developing MPI and for designing MNPs appropriate for MPI.

Acknowledgements

This work was supported by Grants-in-Aid for Scientific Research (Grant Nos.: 25282131 and 15K12508) from the Japan Society for the Promotion of Science (JSPS) and Japan Agency of Science and Technology (JST).

References

[1] Gleich, B. and Weizenecker, J. (2005) Tomographic Imaging Using the Nonlinear Response of Magnetic Particles. *Nature*, **435**, 1214-1217. https://doi.org/10.1038/nature03808

[2] Biederer, S., Knopp, T., Sattel, T.F., Ludtke-Buzug, K., Gleich, B., Weizenecker, J., Borgert, J. and Buzug, T.M. (2009) Magnetization Response Spectroscopy of Superparamagnetic Nanoparticles for Magnetic Particle Imaging. *Journal of Physics D: Applied Physics*, **42**, Article ID: 205007. https://doi.org/10.1088/0022-3727/42/20/205007

[3] Murase, K., Konishi, T., Takeuchi, Y. and Takata, H. (2013) Experimental and Simulation Studies on the Behavior of Signal Harmonics in Magnetic Particle Imaging. *Radiological Physics and Technology*, **6**, 399-414. https://doi.org/10.1007/s12194-013-0213-6

[4] Michels, W.C. and Curtis, N.L. (1941) A Pentode Lock-in Amplifier of High Frequency Sensitivity. *Review of Scientific Instruments*, **12**, 444-447. https://doi.org/10.1063/1.1769919

[5] Murase, K., Hiratsuka, S., Song, R. and Takeuchi, Y. (2014) Development of a System for Magnetic Particle Imaging Using Neodymium Magnets and Gradiometer. *Japanese Journal of Applied Physics*, **53**, Article ID: 067001. https://doi.org/10.7567/JJAP.53.067001

[6] Murase, K., Song, R. and Hiratsuka, S. (2014) Magnetic Particle Imaging of Blood Coagulation. *Applied Physics Letters*, **104**, Article ID: 252409. https://doi.org/10.1063/1.4885146

[7] Rahmer, J., Weizenecker, J., Gleich, B. and Borgert, J. (2009) Signal Encoding in Magnetic Particle Imaging: Properties of the System Function. *BMC Medical Imaging*, **4**, 1-21. https://doi.org/10.1186/1471-2342-9-4

[8] Minard, K.R. and Wind, R.A. (2002) Picoliter ^{1}H NMR Spectroscopy. *Journal of Magnetic Resonance*, **154**, 336-343. https://doi.org/10.1006/jmre.2001.2494

[9] Chikazumi, S. and Charap, S.H. (1964) Physics of Magnetism. Wiley, New York.

[10] Kiss, L.B., Soderlund, J., Niklasson, G.A. and Granqvist, C.G. (1999) New Approach to the Origin of Lognormal Size Distributions of Nanoparticles. *Nanotechnology*, **10**, 25-28. https://doi.org/10.1088/0957-4484/10/1/006

[11] Kluth, T. (2018) Mathematical Models for Magnetic Particle Imaging. *arXiv*, 1-20. https://doi.org/10.1088/1361-6420/aac535

[12] Murase, K., Oonoki, J., Takata, H., Song, R., Angraini, A., Ausanai, P. and Matsushita, T. (2011) Simulation and Experimental Studies on Magnetic Hyperthermia with Use of Superparamagnetic Iron Oxide Nanoparticles. *Radiological Physics and Technology*, **4**, 194-202. https://doi.org/10.1007/s12194-011-0123-4

[13] Reeves, D.B. and Weaver, J.B. (2015) Combined Néel and Brown Rotational Langevin Dynamics in Magnetic Particle Imaging, Sensing, and Therapy. *Applied Physics Letters*, **107**, Article ID: 223106. https://doi.org/10.1063/1.4936930

[14] Murase, K., Shimada, K. and Banura, N. (2016) Correction of Blurring Due to a Difference in Scanning Direction of Field-Free Line in Projection-Based Magnetic Particle Imaging. 6*th International Workshop on Magnetic Particle Imaging*, 16-18 March 2016, Lübeck.

[15] Macias-Bobadilla, G., Rodríguez-Reséndiz, J., Mota-Valtierra, G., Soto-Zarazúa, G., Méndez-Loyola, M. and Garduño-Aparicio, M. (2016) Dual-Phase Lock-in Amplifier Based on FPGA for Low-Frequencies Experiments. *Sensors*, **16**, Article ID: 379. https://doi.org/10.3390/s16030379